Submitted to Particle & Particle Systems Characterization

DOI: 10.1002/ppsc.((please add manuscript number))

Article type: Full Paper

A Correlative Analysis of Gold Nanoparticles Internalized by A549 Cells

*Katharina Böse, Marcus Koch, Christian Cavelius, Alexandra K. Kiemer, and Annette Kraegeloh**

Katharina Böse, Dr. Marcus Koch, Dr. Christian Cavelius, Dr. Annette Kraegeloh

INM - Leibniz Institute for New Materials, Campus D2 2, 66123 Saarbrücken, Germany

E-mail: annette.kraegeloh@inm-gmbh.de

Prof. Dr. Alexandra K. Kiemer

Saarland University, Campus C2 2, 66123 Saarbrücken, Germany

Fluorescently labeled nanoparticles are widely used to investigate nanoparticle cell interactions by fluorescence microscopy. Due to limited lateral and axial resolution, nanostructures (< 100 nm) cannot be resolved by conventional light microscopy techniques. Especially after uptake into cells, a common fate of the fluorescence label and the particle core cannot be taken for granted. Within this study, we present a correlative approach to image fluorescently labeled gold nanoparticles inside whole cells by correlative light and electron microscopy (CLEM). This approach allows for detection of the fluorescently labeled particle shell as well as for the gold core in one sample. In our setup, A549 cells are exposed to 8 nm Atto 647N labeled gold nanoparticles (3.3 10^9 particles ml^{-1}, 0.02 µg Au ml^{-1}) for 5 h and subsequently imaged by confocal laser scanning microscopy (CLSM) and transmission electron microscopy (TEM). Eight fluorescence signals located at different intracellular

positions were further analyzed by TEM. Five of the eight fluorescence spots were correlated with isolated or agglomerated gold nanoparticles. Three fluorescence signals could not be related to the presence of gold, indicating a loss of the particle shell.

1. Introduction

The interactions of nanoparticles with human cells are of great interest with regard to safe handling and application of engineered nanomaterials in various fields including biomedicine.[1] In this context, gold is an important nanomaterial.[2] Current *in vitro* studies focus on uptake mechanisms and the target location of nanoparticles inside different cell types by microscopy.[3] Nanoparticles composed of elements with high atomic number, e.g. gold, are widely used for assessing nanoparticle cell interactions by electron microscopy.[4] However, the preparation of cells for electron microscopy is challenging and time-consuming and may cause shrinking or flattening of the cells or introduction of structural artifacts.[5] On the other hand, fluorescence labels are commonly introduced to enhance the contrast of nanoparticles for studies utilizing advanced fluorescence microscopy techniques, e.g. CLSM.[6] Fluorescence microscopy and suitable preparation techniques enable staining of a wide range of specific cellular structures, multiplex imaging, as well as live cell imaging.[7] In comparison to electron microscopy, fluorescence microscopy provides a larger field of view, but generally suffers from low lateral and axial resolution, making a differentiation between single particles or particle agglomerates difficult.[8]

Correlative light and electron microscopy (CLEM) has the power to combine advantages from both, fluorescence and electron microscopy.[9] CLEM comprises a wide range of potential markers. Most prominent are quantum dots, which emit light at a well-defined wavelength.[10] Their composition, e.g. CdSe or ZnS, simultaneously allows detection by electron microscopy.[11] In other approaches, the production of free radicals from fluorophores is used

to create electron dense precipitates that can be visualized by electron microscopy.[12] Furthermore, fluoronanoprobes are widely used to label cellular structures for CLEM. Small colloidal metal nanoparticles, predominately gold, and fluorophores are conjugated to an antibody, enabling the imaging of cellular structures by fluorescence and electron microscopy.[13] Fluorescently labeled metal nanoparticles are a common particle system to investigate nanoparticle cell interactions by light microscopy. Their similarity to the previously mentioned fluoronanoprobes makes them a suitable substrate for CLEM. There are plenty of publications dealing with fluorescently labeled metal nanoparticles.[14] Generally, this functionalization is realized by a polymer that introduces water solubility and carries the fluorescent dye.[15] Although the nanoparticle shell is believed to influence uptake, intracellular delivery, and toxicity, scientific data regarding the stability of the nanoparticle-polymer-dye complexes in terms of a combined intracellular presence is lacking.[16] It is known that nanoparticles agglomerate in physiological media, if not sufficiently stabilized.[17] Ligand exchange reactions might cause replacement of the original coating.[18] Nanoparticles might be stabilized by binding of proteins to the particle surface forming the so-called protein corona, thus acting as spacer molecules or steric stabilizer.[19] Cellular compartments differ in pH as well as in enzyme and protein composition from the extracellular environment. These factors have already been shown to affect nanoparticle stability.[20] The uptake of gold nanoparticles by epithelial cells has been studied recently by combining dark-field light microscopy and transmission electron microscopy (TEM).[21] Up to now there is no correlative microscopic study examining the location of fluorophores as markers for the particle coating compared to the particle core, especially after their uptake into cells. Within this study, we report the application of CLEM to monitor fluorescently labeled polymer coated gold nanoparticles inside A549 cells using CLSM and TEM. The focus of this study is on the spatial correlation of the fluorescence and the respective gold signals. For cell

culture, silicon nitride microchips were used as they have already been shown to be a suitable substrate for imaging whole cells by fluorescence and electron microscopy.[22] Whole cells were prepared for TEM based on the dehydration of cells at a pressure below the equilibrium vapor pressure of water.[23]

2. Results

2.1. Properties of gold nanoparticles

By use of TEM, the morphology and size of the fluorescently labeled gold nanoparticles was determined. The particles were roughly spherical with a diameter of 8.4 nm +/- 0.5 nm (Figure 1a). Hence, the nanoparticles were designated as 8 nm in size. The presence of the polymer coating surrounding the nanoparticles was monitored by depositing the particle dispersion on a holey carbon film. For gold nanoparticles laying at the edge of the carbon film, the polymer shell could be visualized by TEM analysis (Figure 1b). A shell thickness of ~1 nm was determined, resulting in a total particle diameter of about 10 nm. This data was in accordance with DLS measurements, indicating a hydrodynamic particle diameter of 13.2 nm ± 4.8 nm. TEM micrographs of gold nanoparticles without polymer shell are included in the supporting information (Figure S1). Due to the large number of carboxyl groups on the polymer shell, the particles exhibited a strongly negative zeta potential (-49.7 mV). The physico-chemical parameters of the gold nanoparticles are summarized in Table 1. The particle dispersion exhibited an absorption maximum at 520 nm due to the surface plasmon resonance. The absorption maximum did not significantly shift after dispersion of the particles in cell culture medium, indicating particle stability under these conditions. UV-Vis and emission spectra of fluorescently labeled gold nanoparticles are included in the supporting information (Figure S2) as well as EDX analyses of the gold particles on silicon nitride chips

(Figure S3). After phase transfer and labeling, the particles were purified by repeated centrifugation steps to remove unbound dye and polymer molecules.

2.2. Localization of Atto 647N fluorescence signals by CLSM

After exposition of A549 cells to Atto 647N-labeled gold nanoparticles and sample preparation, cell samples were analyzed with regard to Atto 647N fluorescence signals using CLSM. Most of the observed cells exhibited signals related to Atto°647N, although the number of fluorescent spots per cell varied between cells. Typically, Atto 647N signals were distributed in a punctate pattern and accumulated in the perinuclear region of the cells, as can be seen from the image given in Figure S4. The correlative analysis described in the following was conducted on eight Atto 647N signals present in one cell (**Figure 2a**). Two further signals within adjoining cells were also analyzed (data not shown). For correlative analysis, the tubulin cytoskeleton was used as a cellular marker. Microtubules radiate from the centrosome throughout the cell and extend to the plasma membrane, to which they are attached by protein linkers.[24] Microtubules were therefore also used to indicate the cellular boundaries. In order to determine the three-dimensional distribution of the fluorescence signals, confocal z-stacks were recorded. Orthogonal sections indicated that the Atto 647N signals were located inside of the cell, as shown for positions 4 and 8 (**Figure 3**). Using the information on the z-positions of the Atto 647N signals, their distances to the upper and lower margin of the cell were determined (Table S1).

2.3. Correlative imaging of cell samples by electron microscopy

After analysis by CLSM, A549 cells were post-fixed with glutaraldehyde. Samples were then transferred to the SEM and imaged in transmission mode by wet scanning transmission electron microscopy (wet STEM) in a water containing atmosphere (750 Pa, 276 K) at E = 30 keV. Using the wet STEM mode, the cell previously analyzed by confocal microscopy was identified based on its shape (Figure S5a). The nucleus appeared as the dark central region, but further details of the cellular structure were not readily identifiable as the cell had not been treated with contrast enhancing agents like osmium tetroxide during the preparation. At higher magnification, dark spots were detected within the nuclear region, but appeared only weakly (Figure S5b). For a clearer image, the pressure was reduced to 720 Pa (Figure S5c). Single nanoparticles could not be resolved, due to the limited acceleration voltage (Emax = 30 keV). In addition, under these conditions, EDX measurements could not be applied to identify the composition of the dark spots. Immediately after imaging, the samples were dried within the ESEM chamber, applying an even lower pressure as described in the experimental section. Dehydrated samples were subsequently transferred to the TEM. The cell analyzed by CLSM was identified and imaged (Figure 2b). Besides the nucleus, lamellar bodies contained within A549 cells were clearly visible. Due to the mass-thickness contrast, they appeared as dark circular structures with sizes in the range of 0.6 - 1.2 µm. Similar to the maximum intensity projection (Figure 2a), three cells were identified whereas one cell was completely visible in the center of the image. Within the cell adjacent to the right, nucleus and lamellar bodies were also visible. In the electron micrograph, the border between the two cells was allocated according to the dark line between them. This border correlated with the region between the cells in the fluorescence image, containing a less dense microtubule network (Figure 2a). In the electron micrograph, thin connections between the central cell and the cell adjacent to the left were visible, not crossed by microtubules. Nevertheless, the cell margin of

the central cell was visible in both images (Figure 2a and 2b) and was used to superimpose the maximum intensity projection with the TEM micrograph. The overlay of TEM and CLSM images based on the cell shape has been reported as a suitable method for correlative microscopy.[25] The positions of nucleus and lamellar bodies were also used to align both images. Although less pronounced in the maximum intensity projection shown in Figure 2c, in two-dimensional confocal images, the nucleus and lamellar bodies were indicated by a less dense microtubule network (Figure 3).

As mentioned above, eight Atto 647N fluorescence signals were chosen on the basis of the maximum intensity projection for further analysis by electron microscopy (Figure 2a). Their positions were transferred to the TEM image (Figure 2d), defining the regions for the TEM analyses. The results are exemplified in detail for two signals only. The signal at position 4 was chosen, because it exhibited the brightest fluorescence compared to the signals at the other seven positions. The analysis of the z-stacks revealed that it resided in the inner region of the cell (Table S1). As indicated by TEM, position 4 was in an electron dense region containing part of the nucleus. In comparison, the fluorescence signal at position 8 was much less intense and closer to the apical side of the cell (Table S1). TEM analysis indicated that it resided in a less electron-dense region beside of the nucleus.

2.4. Correlation of fluorescence signals with positions of gold nanoparticles

In order to detect gold nanoparticles, series of TEM images were taken with increasing magnification (**Figure 4** and **Figure 5**). Gold nanoparticles were detected from a magnification corresponding to an image size of 2 µm x 2 µm. At position 4, eleven gold nanoparticles were detected within a distance of 140 nm (Figure 4f). Within 40 nm, seven particles formed an agglomerate close to a further single one. The other three particles resided in a distance of about 100 nm from the agglomerate. The size and shape of the particles was in

accordance with the properties as determined in the cell-free system. At position 8, two single gold nanoparticles were detected in a distance of 55 nm. These particles were 3 nm and 6 nm in diameter, which was below the calculated mean diameter (Table 1). However, EDX measurements confirmed that the particles consisted of gold (Figure S6).

Similarly, TEM zoom series were taken at the other six positions indicated in Figure 2a. Gold nanoparticles could be detected at a magnification corresponding to an image size of 2 µm x 2 µm. At five out of eight positions, gold nanoparticles were detected by TEM analysis (Figure S7). At the other three positions, gold nanoparticles were not detected within an area of 2 µm x 2 µm surrounding the fluorescence signal.

As specified in Figure S7, the number of gold particles at each position and the intensity of the fluorescence signals were determined from the TEM and confocal images. Interestingly, the fluorescence intensity at position 4 was five to ten times higher than the intensity measured at the other positions. At the same position, a multiple (four- to eleven-fold) number of gold nanoparticles was determined as compared to the other positions. Nevertheless, a quantitative relation between the number of gold nanoparticles and the fluorescence intensity could not be derived, due to a lack of positions exhibiting an intermediate number of gold nanoparticles.

Finally, the distances between the correlative fluorescence signals and gold nanoparticles were determined (**Table 2**). Therefore, the location of the gold nanoparticles was transferred into the fluorescence images (**Figure 6**). As the gold nanoparticles were only resolved at higher magnification, their positions were related to markers also present at lower magnification. The particles at inner positions (3, 4, and 6) were correlated with the margin of adjacent lamellar bodies. The particles at outer positions were related to the cell margin (position 1) and NaCl containing precipitates (position 8).

The distances between the fluorescence signals at positions 1 and 8 located within the outer part of the cell and the gold particles were 830 nm and 610 nm. The particles located at inner positions exhibited lower distances to the fluorescence signals (110 - 390 nm). The precision of the given distances (Table 2) was dependent on the size of the marker and corresponded to the length of one (50 nm) and four pixel (200 nm) in the TEM images (e.g. Figure 4c and Figure 5c). For an evaluation of these values, the limited resolution of conventional confocal microscopy (~300 nm at the imaging conditions used) has to be taken into account.

3. Discussion

3.1. Particle dosage for microscopic studies on nano cell interactions

The uptake of nanoparticles into cells is an active research topic with relevance for nanobiomedicine as well as nanotoxicology.[26] The intended administration of nanoparticles for biomedical applications such as contrast agents facilitates an accurate estimation of the applied dose. In contrast, many *in vitro* as well as *in vivo* studies in the field of nanotoxicology are considered to exceed relevant exposure conditions.[27] In addition, incomplete characterization data hamper a comparison between studies, in particular between toxicological and microscopy investigations. In this study, the cells were exposed to a concentration of 0.02 µg Au ml^{-1}, corresponding to 0.1 µmol Au l^{-1}. This low concentration was chosen to exclude nanoparticle-induced cytotoxicity, potentially affecting uptake and target location of the particles. At the concentration chosen as well as at higher concentrations (up to 2 µg Au ml^{-1}), no particle-induced cytotoxicity was observed, applying a conventional cytotoxicity assay (WST-1, data not shown). Generally, gold nanoparticles exhibit a cytotoxic potential at high doses, which is dependent on surface charge, surface coating, and particle exposure time.[28] In comparison to other microscopy studies (Table S2), the cells were

exposed to a significantly lower gold or particle concentration, in order to approach a more realistic exposure scenario corresponding to the cell type used. The narrow size distribution of the gold nanoparticles allowed calculating the number of particles at the applied concentration, accounting to $3.3°10^9$ particles ml^{-1} or a molar particle concentration of 0.0055 nM. In other studies (Table S2), the cells were exposed to a 15 - 500-fold particle concentration. The concentration used here, corresponded to 1.9 - 3.9 10^4 nanoparticles per cell in five hours. Considering the liquid column above the cells (~3 mm), the cells residing within the lower 100 µm of this column were exposed to an average of 600 - 1,300 nanoparticles. The order of magnitude of these numbers corresponded well to 120 - 2,400 particles per hour calculated by Geiser et al. to maximally encounter one alveolar cell after inhalation.[29]

It seems that for microscopic studies, high particle concentrations are gladly chosen to facilitate detection of particles within the cellular environment. We recommend considering potential cytotoxic effects induced by high nanoparticle concentrations and relevant exposure doses for microscopic studies on nanoparticle cell interactions. Besides nanoparticle functionalization, the low dosage used in this study is one explanation for the detection of separated particles as well as separated particle agglomerates within the cells. Single particles and agglomerates have also been found by Brandenberger using A549 cells.[3] In contrast using other cell types, Peckys et al. observed particle filled vesicles within the cells and Freese et al. detected particle agglomerates as black dots in the perinuclear region even by light microscopy.[30]

3.2. The use of CLEM for investigating nanoparticle cell interactions

Beside of the dose, parameters like particle size, shape, and surface modification are regarded to determine uptake and the intracellular fate of particles after uptake.[16] Especially, surface modification and functionalization of particles are important, influencing particle stability,

specific uptake or intracellular targeting beyond the endosomal compartment.[31] Microscopy methods can provide insights into nanoparticle uptake and transport and are therefore a valuable tool for a quantification of nanoparticle cell interactions.[32] Most microscopy techniques suitable for the cellular environment enable either the detection of the particle core or the detection of the surrounding shell. In contrast, correlative microscopy facilitates spatial information on both components, even after internalization by cells. In our study, CLEM was used to analyze the presence of gold cores in comparison to the fluorescently labeled particle shell inside A549 cells. Only five out of eight fluorescent spots correlated with gold particles, suggesting detachment of the fluorescent dye or the polymer shell from the particle core. Reasons for the release of fluorescent dyes or drugs from nanoparticles are manifold and strongly depend on their chemical properties and on the chemical bond to the particle matrix or surface. Nonpolar dyes are for example used to label the matrix of polystyrene nanoparticles, simply by embedding. Once in contact with cells, release of dyes has been observed.[33] Dye release has also been shown for particles labeled with a dye covalently attached to the polymeric particle matrix. In this case, significant leaching from particles, which had been subjected to dialysis prior to cell experiments, appeared to have caused a strong background in fluorescence microscopy.[34] A significant background due to leaching of free Atto 647N was not observed during this study. The dye was covalently attached to the polymer used for phase transfer of the particles into the water phase and for electrosteric stabilization of the particles. The polymer itself was attached *via* van der Waals and hydrophobic forces to alkylthiols anchored to the particle surface via semi-covalent, high affinity thiol-gold bonds. TEM analyses of the nanoparticles at the edge of a holey carbon film demonstrated the presence of the polymer coating around the gold core. As the alkylthiol covered particles lacking the polymer shell are not stable in water, we assume that a detachment of the polymer occurred after transfer of the particles to the cell culture medium

or after uptake into the cells and that this was responsible for the reduced correlation between fluorescence signals and gold nanoparticles.[15] It is well known that in biological environment a protein corona is formed around nanoparticles.[16] As after transfer into cell culture medium, a blue shift of the absorption maximum of the particles, indicating particle agglomeration, was not observed (data not shown), we assume that proteins with a high affinity to the particle surface or the covalently bound alkyl-linker molecules might have replaced the polymer shell gradually.[35] An unspecific staining of cellular structures as has been described for mitochondrial membranes by Atto 647N antibody conjugates or for the endoplasmic reticulum by unpolar dyes was also not observed, indicating that the polymer complexes do not freely diffuse throughout the cells.[33, 36] Nanoparticles are regarded to be taken up into the endolysosomal compartment of various cell types.[33] Destabilization of particle polymer complexes might be caused by the low pH present in these compartments or by enzymatic cleavage.[20, 37]

The more detailed TEM analysis of position 4 and 8 suggested a relationship between the fluorescence intensity and the number of gold particles present. Nevertheless, no proportional relationship between the fluorescence intensity and the number of gold nanoparticles at the other positions was found. The number of fluorophores per particle was calculated by comparison of the fluorescence of the particle dispersion compared to a solution of free Atto 647N. Statistically, every gold nanoparticle carried 23 ± 4 molecules of Atto 647N attached to the polymer. The standard deviation from this value is expected to be mainly influenced by the coupling efficiency of mPEG and the fluorophore itself, which are both coupled to free carboxylic acid residues on the PMAO backbone.

The lack of correlation between the fluorescence intensity and the number of correlating gold particles can also be explained by the limited sensitivity of CLSM at the applied conditions. The slight refractive index mismatch and the accompanying light reflection might cause a

decreased fluorescence yield. Additionally, the absence of antifading reagents might have promoted photobleaching of the fluorescent dye. Thus, part of the nanoparticle derived fluorescence was possibly lost during analysis.

Regardless of the complexity of potential explanations for the imperfect correlation, more than half of the spots exhibited a correlation between the fluorescence signal and the presence of gold particles, indicating that these particles retained the shell during uptake into the cells. Such kind of information provided by CLEM is important for biomedical targeting approaches, relying on the surface modification of nanoparticles, e.g. particle delivery to the nucleus as well as in the context of a safer design of nanoparticles.[31] Beside of polymers, the fate of proteins initially bound to the particle surface can be investigated by this technique. The applicability of fluorescence microscopy for localization of labeled particles should be tested, especially when the used label is coupled to the particle surface. In addition, the restricted resolution of conventional light microscopy might not easily allow the actual localization of nanostructures.[8] In comparison to light microscopy, TEM allows for identification of the elemental composition of a sample. In this study, EDX measurements were applied to identify a single gold nanoparticle located inside the cell. Without such measurements, other structures, e.g. caused by the preparation procedure, might be misinterpreted. Furthermore, single nanoparticles located in deeper regions (~5 µm) of the cell were detectable by TEM down to a size of 3 nm. Similar results were obtained by de Jonge et al., resolving 10 nm gold particles inside whole liquid cells by scanning TEM.[38] In this study, the gold nanoparticle agglomerate at position 4 was located in the middle of the cell underneath the nucleus as indicated by CLSM (Figure 3a). Although the electron beam is scattered on its way through the cell, individual gold nanoparticles were clearly resolved by TEM (Figure 4f).

3.3. Influence of sample preparation on CLEM

The imaging of cells by electron microscopy usually requires a complete dehydration of the cellular material. Examples of techniques enabling imaging of hydrated samples are cryo-electron microscopy, environmental SEM (ESEM) including wet STEM imaging, and liquid STEM.[22, 39] However, under the conditions used here, wet STEM imaging was not sufficient for the identification of 8 nm intracellular nanoparticles. Therefore, the sample was dehydrated for a further analysis by TEM. Dehydration of biological material can be achieved by critical point drying or air drying after treatment of the sample with fluids of low surface tension. Such treatment of cells is often accompanied by cell shrinkage introducing artifacts.[40] In the present study, the dehydration of cells was realized inside an ESEM chamber at a temperature of 276 K and a pressure of 600 Pa, which is below the equilibrium vapor pressure. It has been described that under these conditions, the moisture loss of hydrated specimen proceeds slowly, preventing a massive sample shrinkage.[23] The recorded TEM images indicated no significant changes in the lateral dimensions of the cell, allowing for superimposition of the maximum intensity projection and electron micrographs. The cell boundaries, visible in both images, matched well. Sample shrinkage in axial direction was observed after imaging of the dried cells by scanning electron microscopy using different tilt angles (data not shown). By the correlative analysis at five out of eight fluorescence spots gold nanoparticles were detected, indicating preservation of the particle location after drying. Especially at positions 3, 4, and 6, located in the center of the cell, the fluorescence signals and the gold particles were close to each other. The distances were less than 400 nm, a value similar to the optical resolution of fluorescence microscopy. At positions 1 and 8, closer to the cell borders, a poorer match of Atto 647N fluorescence and gold nanoparticles was observed (< 830 nm, Table 2). Nevertheless, the positions of the gold particles detected could be linked to the observed fluorescence as no other gold nanoparticles were found in spatial proximity

(within 2 µm x 2 µm). The area investigated by TEM comprised ~3°% of the total cell area. Thus, we cannot exclude the presence of gold cores that had separated from the shell in the remaining area. We do not assume that sample preparation caused the loss of the gold cores from the fluorescent shells, because after CLSM, the cells were only post-fixed using glutaraldehyde and directly transferred to the ESEM chamber to allow drying of the sample. No dehydration by solvent exchange was carried out, potentially causing flushing of nanoparticles. As discussed in section 3.2, the absence of gold particles can more likely be related to a loss of the Atto 647N labeled polymer from the gold core during contact of the particles to biological components.

4. Conclusion

A549 cells as model for human alveolar epithelial cells were exposed to 8 nm Atto 647N labeled gold nanoparticles for 5 h and analyzed by CLEM. The cells were exposed *in vitro* to gold particles at a low concentration relevant for an inhalative nanoparticle uptake. Atto 647N signals were detected by CLSM allowing for a diffraction-limited determination of their three-dimensional position within the cells. Eight of these signals were chosen for further correlative analyses by TEM. Five of the fluorescence signals correlated with single gold nanoparticles or nanoparticle agglomerates. This correlative approach allowed for a detection of fluorescence signals in three dimensions using whole cells complemented by detection of single or agglomerated gold particles within or close to the diffraction limited fluorescent spots. Our study indicated that the polymer shell was lost from three out of eight gold nanoparticles. CLEM appears to be very powerful in the analysis of nano cell interactions and the intracellular distribution of particle cores relative to the particle shell.

5. Experimental Section

Gold nanoparticles: 8 nm lipophilic dodecanthiol-capped gold nanoparticles were prepared according to the method described by Zheng et al.[41] Particles were transferred into water using a modified phase transfer protocol described by Pellegrino.[15] Labeling of the polymer coated particles with Atto 647N dye was achieved through activation of carboxylate groups on the particle surface with N-(3-dimethylaminopropyl)-N′-ethylcarbodiimide (EDC) / N-hydroxysuccinimide (NHS) and further reaction with amine-modified Atto 647N-NH_2. Further details on the particle preparation and particle characterization are given in the Supporting information.

Cell culture: The human lung carcinoma cell line A549 (ACC 107) as model for type II alveolar epithelial cells was used within this study.[42] The cells were obtained from the German Collection of Microorganisms and Cell Culture (DSMZ, Braunschweig, Germany). A549 cells were grown in Dulbecco's modified eagle's medium (DMEM) (Gibco, Life Technologies, USA) supplemented with 10 % (v/v) fetal bovine serum (FBS) (PAN biotech, Germany) at 37 °C in a 9 % CO_2 atmosphere. After reaching ~80 % confluence, cell cultures were split using 0.05 % trypsin containing 0.02 % EDTA (PAN biotech, Germany). For experiments, cells from passage 20 were used.

Preparation of silicon nitride microchips and cell seeding: Custom made silicon nitride microchips (Protochips, Hummingbird, USA) were kindly provided by Protochips Inc. These microchips were used as substrates for cell culture and correlative microscopy. The chips feature a 50 x 400 μm^2 window with a thickness of 50 nm allowing transmission of the laser as well as the electron beam and are therefore suited for both, fluorescence and electron microscopy. Prior to cell seeding, the microchips were cleaned as published previously.[30a] The cleaned chips were transferred into a 96-well plate. Each well (area: 34 mm^2) was filled with 100 µl of cell culture medium and A549 cells were seeded onto the chips. An appropriate

cell density of 5 - 10 cells per window (8.500 - 17.000 cells per well) was determined experimentally. DMEM without phenol red (PAN biotech, Germany) supplemented with 10 % (v/v) FBS was used as cell culture medium. Prior to nanoparticle exposure, the cells were incubated for 20 - 24 h to allow cell attachment.

Exposure of cells to nanoparticles: Dispersions of 0.02 µg Au ml^{-1}(3.9 10^9 particles ml^{-1}) were prepared freshly prior to each experiment by diluting the nanoparticle stock in cell culture medium. The colloidal dispersions were mixed using a vortex mixer and added to A549 cells grown on silicon nitride microchips. The cells were exposed to gold nanoparticles for 5 h. The total particle number in the applied volume was 3.3 10^8.

Immunostaining: The tubulin cytoskeleton of A549 cells was fluorescently labeled using antibodies using standard techniques. A detailed description of the staining protocol is given in the Supporting information.

Confocal microscopy: The Leica TCS SP5 system with a 100x/1.4 oil immersion objective (HCX PL APO, Leica, Germany) was used for confocal imaging. Prior to microscopic analyses, the chips were transferred into cell view dishes equipped with a glass bottom (Greiner BioOne, Germany) and placed upside down onto the glass. After addition of 500 µl PBS, the samples were imaged immediately. Atto 647N was excited by using a HeNe laser with an excitation wavelength of 633 nm. An avalanche photodiode (APD) was used to detect the emitted fluorescence. Alexa 488-labeled α-tubulin was imaged using an argon laser line of 488 nm for excitation. The fluorescence emission was detected by a photomultiplier tube (PMT). The pinhole size was set to 1 AU. Images and z-stacks were recorded sequentially. A z-step size of 130 nm and pixel sizes of 50 - 70 nm^2 were chosen.

Scanning transmission electron microscopy of hydrated samples in the ESEM (wet STEM) and transmission electron microscopy (TEM): After confocal imaging, cells were additionally fixed with 1 % (v/v) glutaraldehyde (Electron microscopy science, UK) and rinsed with PBS.

Samples were stored in PBS at 277 K. Prior to imaging, samples were briefly washed in water and mounted on a pre-cooled wet STEM sample holder (T = 276 K). Subsequently, samples were transferred into the chamber of an ESEM Quanta 400 FEG (FEI Company, Hillsboro, USA) microscope. In order to exchange the ambient atmosphere for an atmosphere, containing water at imaging conditions, the ESEM chamber was purged with water vapor five times using a pressure range of 800 - 1,500 Pa. Imaging was performed at 750 and 720 Pa and 30 keV (spot size 3) using a solid-state detector in the bright field mode for the collection of transmitted electrons. At 750 Pa and T = 276 K, water is at the phase boundary between liquid and gaseous water, according to the p-T phase diagram.[23] Thus, we assume that the cells were in a fully hydrated state. At 720 Pa, the equilibrium is shifted just below the phase boundary. After imaging for about 10 min, the pressure in the ESEM chamber was reduced to 600 Pa for further 10 min. Under these conditions, water is in its gaseous phase, allowing for dehydration of the cells.[23] Subsequently, samples were transferred to a TEM sample holder and investigated at room temperature using a Philips CM200 FEG (FEI Company, Eindhoven, NL) at 200 keV (gun lens 2, spot size 1) equipped with a MultiScan camera (Model 794, Gatan, Pleasanton, USA) and an EDX spectrometer (EDAX DX-4/Phönix, Ametek, Germany). An inherent property of the CM200 comprises automatic image rotation with increasing magnification. To facilitate superimposition with confocal images, the obtained images were back-rotated.

Image processing: Confocal z-stacks were deconvolved with Huygens professional software (SVI, Netherlands) using the classic maximum likelihood estimation algorithm. Experimentally determined pointspread functions (PSFs) were used for deconvolution. For illustrations, intensity measurements, and orthogonal sectioning, images and stacks were further processed in Fiji.[43]

Supporting Information

Supporting Information is available online from the Wiley Online Library or from the author.

Acknowledgements

The authors thank Diana Peckys for help with the usage of silicon nitride microchips during the initial phase of the experiments and Protochips Inc. for providing silicon nitride microchips. The authors thank Henrike Peuschel and Niels de Jonge for useful discussions. The authors also thank Eduard Arzt for ongoing support of their work at INM. The authors acknowledge funding of part of this work by Saarland Ministry of Economics and Research (LFFP 05/06).

Received: ((will be filled in by the editorial staff))

Revised: ((will be filled in by the editorial staff))

Published online: ((will be filled in by the editorial staff))

[1] a) G. Oberdörster, *J. Intern. Med.* **2009,** *267*, 89; b) A. Kumar, H. Ma, X. Zhang, K. Huang, S. Jin, J. Liu, T. Wei, W. Cao, G. Zou, X.-J. Liang, *Biomaterials* **2012,** *33*, 1180.

[2] K. Weintraub, *Nature* **2013,** *495*, S14.

[3] C. Brandenberger, C. Mühlfeld, Z. Ali, A.-G. Lenz, O. Schmid, W. J. Parak, P. Gehr, B. Rothen-Rutishauser, *Small* **2010,** *6*, 1669.

[4] P. Nativo, I. A. Prior, M. Brust, *ACS Nano* **2008,** *2*, 1639.

[5] C. Mühlfeld, B. Rothen-Rutishauser, D. Vanhecke, F. Blank, P. Gehr, M. Ochs, *Part Fibre Toxicol* **2007,** *4*, 11.

[6] J. A. Kim, C. Aberg, A. Salvati, K. A. Dawson, *Nat. Nanotechnol.* **2012,** *7*, 62.

[7] N. C. Shaner, G. H. Patterson, M. W. Davidson, *J. Cell Sci.* **2007,** *120*, 4247.

[8] T. Müller, C. Schumann, A. Kraegeloh, *ChemPhysChem* **2012,** *13*, 1986.

[9] B. N. G. Giepmans, *Histochemistry and Cell Biology* **2008,** *130*, 211.

[10] A. P. Alivisatos, W. Gu, C. Larabell, *Annu. Rev. Biomed. Eng.* **2005,** *7*, 55.

[11] B. N. Giepmans, T. J. Deerinck, B. L. Smarr, Y. Z. Jones, M. H. Ellisman, *Nat Methods* **2005,** *2*, 743.

[12] M. Grabenbauer, W. J. C. Geerts, J. Fernadez-Rodriguez, A. Hoenger, A. J. Koster, T. Nilsson, *Nat. Methods* **2005,** *2*, 857.

[13] T. Takizawa, J. M. Robinson, *J Histochem Cytochem* **2000,** *48*, 481.

[14] C. Röcker, M. Pötzl, F. Zhang, W. J. Parak, G. U. Nienhaus, *Nat. Nanotechnol.* **2009,** *4*, 577.

[15] T. Pellegrino, L. Manna, S. Kudera, T. Liedl, D. Koktysh, A. L. Rogach, S. Keller, J. Rädler, G. Natile, W. J. Parak, *Nano Lett.* **2004,** *4*, 703.

[16] A. E. Nel, L. Mädler, D. Velegol, T. Xia, E. M. V. Hoek, P. Somasundaran, F. Klaessig, V. Castranova, M. Thompson, *Nat. Mater.* **2009,** *8*, 543.

[17] C. Schulze, A. Kroll, C.-M. Lehr, U. F. Schäfer, K. Becker, J. Schnekenburger, C. Schulze Isfort, R. Landsiedel, W. Wohlleben, *Nanotoxicol* **2008,** *2*, 51.

[18] D. Mahl, C. Greulich, W. Meyer-Zaika, M. Koller, M. Epple, *J. Mater. Chem.* **2010,** *20*, 6176.

[19] E. Casals, T. Pfaller, A. Duschl, G. J. Oostingh, V. Puntes, *ACS Nano* **2010,** *4*, 3623.

[20] M. Raoof, S. J. Corr, W. D. Kaluarachchi, K. L. Massey, K. Briggs, C. Zhu, M. A. Cheney, L. J. Wilson, S. A. Curley, *Nanomedicine* **2012,** *8*, 1096.

[21] C. Rosman, S. Pierrat, A. Henkel, M. Tarantola, D. Schneider, E. Sunnick, A. Janshoff, C. Sönnichsen, *Small* **2012,** *8*, 3683.

[22] N. de Jonge, D. B. Peckys, G. J. Kremers, D. W. Piston, *Proc Natl Acad Sci* **2009,** *106*, 2159.

[23] D. J. Stokes, *Principles and Practice of Variable Pressure/Environmental Scanning Electron Microscopy (VP-ESEM)*. John Wiley & Sons Ltd: Chichester, 2008.

[24] M. Bifulco, *Proc Natl Acad Sci* **2002,** *99*, 1807.

[25] D. R. Keene, S. F. Tufa, G. P. Lunstrum, P. Holden, W. A. Horton, *Microsc. Microanal.* **2008,** *14*, 342.

[26] F. Zhao, Y. Zhao, Y. Liu, X. Chang, C. Chen, Y. Zhao, *Small* **2011,** *7*, 1322.

[27] H. F. Krug, P. Wick, *Angew. Chem. Int. Ed.* **2011,** *50*, 1260.

[28] N. Lewinski, V. Colvin, R. Drezek, *Small* **2008,** *4*, 26.

[29] M. Geiser, W. G. Kreyling, *Part Fibre Toxicol* **2010,** *7*, 2.

[30] a) D. B. Peckys, N. de Jonge, *Nano Lett.* **2011,** *11*, 1733; b) C. Freese, M. I. Gibson, H.-A. Klok, R. E. Unger, C. J. Kirkpatrick, *Biomacromolecules* **2012,** *13*, 1533.

[31] R. Lévy, U. Shaheen, Y. Cesbron, V. Sée, *Nano Rev* **2010,** *1*.

[32] T. Elsaesser, *Nanomedicine* **2010,** *5*, 1447.

[33] A. Salvati, C. Åberg, T. dos Santos, J. Varela, P. Pinto, I. Lynch, K. A. Dawson, *Nanomed. Nanotechnol. Biol. Med.* **2011,** *7*, 818.

[34] T. Tenuta, M. P. Monopoli, J. Kim, A. Salvati, K. A. Dawson, P. Sadin, I. Lynch, *PLoS ONE* **2011,** *6*, e2556.

[35] Z.-J. Zhu, R. Tang, Y.-C. Yeh, O. R. Miranda, V. M. Rotello, R. W. Vachet, *Anal. Chem.* **2012,** *84*, 4321.

[36] C. A. Wurm, D. Neumann, R. Schmidt, A. Egner, S. Jakobs, *Methods in molecular biology* **2010,** *591*, 185.

[37] V. See, P. Free, Y. Cesbron, P. Nativo, U. Shaheen, D. J. Rigden, D. G. Spiller, D. G. Fernig, M. R. White, I. A. Prior, M. Brust, B. Lounis, R. Levy, *ACS Nano* **2009,** *3*, 2461.

[38] N. d. Jonge, D. B. Peckys, G. J. Kremers, D. W. Piston, *Proceedings of the National Academy of Sciences* **2009,** *106*, 2159.

[39] a) L. F. Kourkoutis, J. M. Plitzko, W. Baumeister, *Ann Rev Mater Res* **2012,** *42*, 33; b) A. Bogner, G. Thollet, D. Basset, P. H. Jouneau, C. Gauthier, *Ultramicroscopy* **2005,** *104*, 290.

[40] M. V. King, *Cell Biophys.* **1991,** *18*, 31.

[41] N. Zheng, J. Fan, G. D. Stucky, *J. Am. Chem. Soc.* **2006,** *128*, 6550.

[42] M. Lieber, B. Smith, A. Szakal, W. Nelson-Rees, G. Todaro, *Int. J. Cancer* **1976,** *17*, 62.

[43] J. Schindelin, I. Arganda-Carreras, E. Frise, V. Kaynig, M. Longair, T. Pietzsch, S. Preibisch, C. Rueden, S. Saalfeld, B. Schmid, J. Y. Tinevez, D. J. White, V. Hartenstein, K. Eliceiri, P. Tomancak, A. Cardona, *Nat Methods* **2012,** *9*, 676.

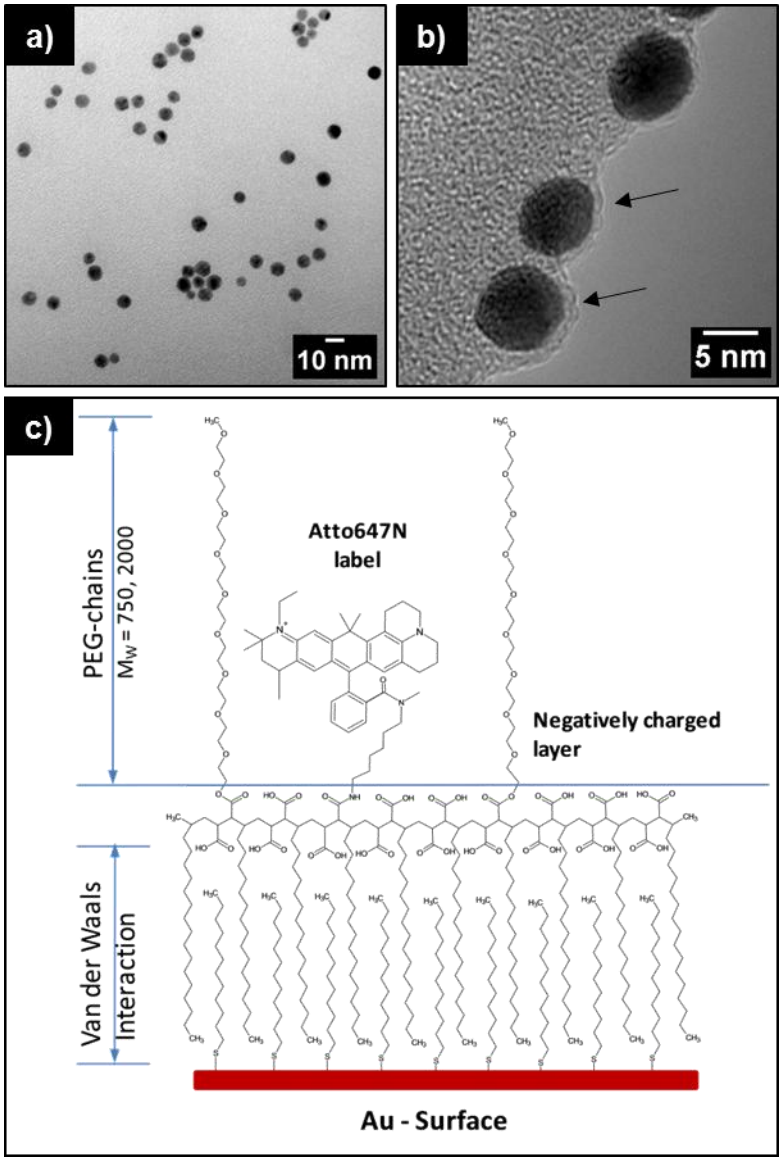

Figure 1. TEM micrographs of Atto 647N labeled gold nanoparticles and scheme of the particle shell.

a) The 8 nm gold nanoparticles showed a narrow size distribution and were well dispersed as indicated by the distances between adjacent particles. b) The polymer coating surrounding the particle surface was visualized at the edge of a carbon film (see arrows). c) Scheme of the functionalized particle surface. Alkylthiol linkers were covalently bound to the nanoparticle surface (Au, red). An amphiphilic polymer (Poly-maleic anhydride–alt octadecene, coupled to mPEG750) was bound via Van der Waals interactions to the linker molecules. Negatively

charged carboxyl groups were used to covalently attach the amine-modified Atto 647N-NH_2 (Atto-Tech, Germany) to the polymer surface.

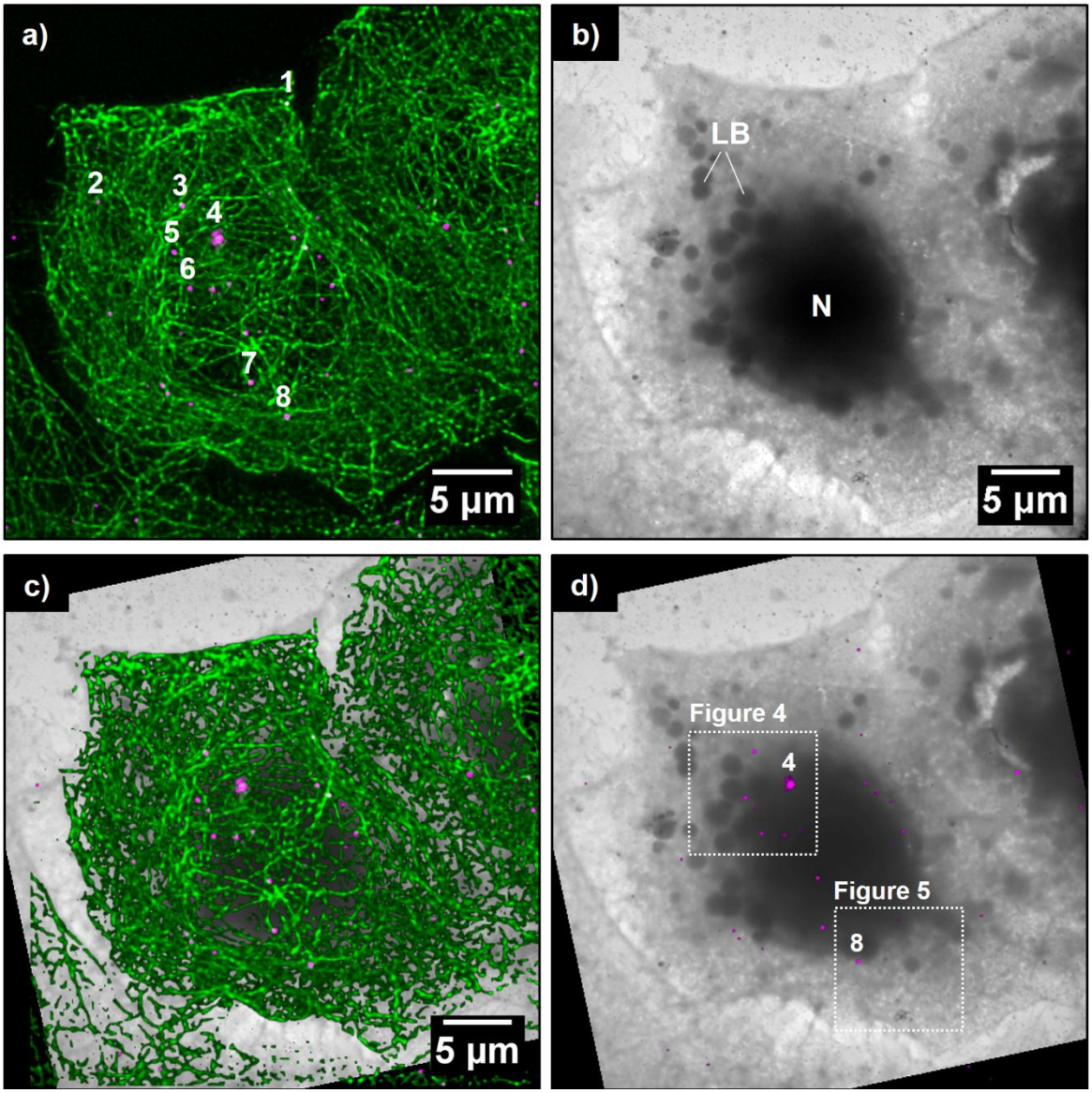

Figure 2. Correlative imaging of one and the same cell by confocal microscopy and TEM. a) Maximum intensity projection of the deconvolved confocal z-stack (green: α-tubulin, magenta: Atto 647N). b) Corresponding TEM image showing the nucleus (N) and lamellar bodies (LB). c) Overlay of the maximum intensity projection and the TEM image. To facilitate superimposition, the TEM image b) was rotated. Correlation of both images was achieved by comparison of morphological features, mainly the cell edges. d) Overlay of the TEM image and Atto 647N signals (magenta). The contrast of the TEM image was adjusted to improve visibility of the Atto 647N signals in the overlay. Eight fluorescent spots (positions 1 - 8 in a) were analyzed by CLEM. Positions 4 and 8 were chosen as examples to

illustrate further analysis (see Figure 4 and Figure 5). The squares in d correspond to Figures 4a and 5a and represent the start images of TEM analyses.

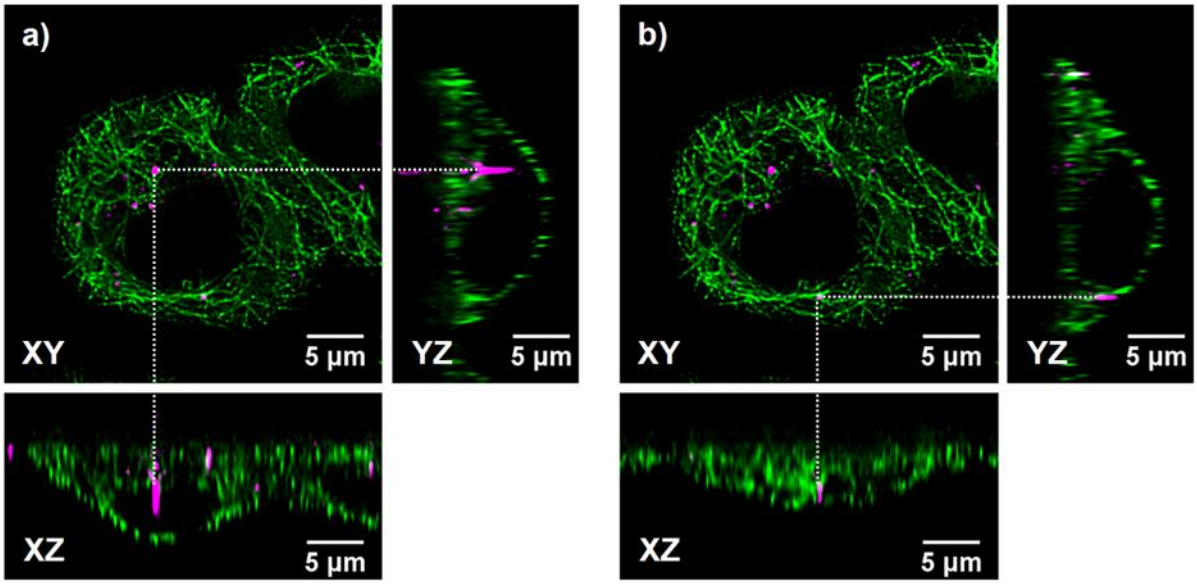

Figure 3. Localization of Atto 647N signals inside A549 cells using CLSM. The cells were exposed to Atto 647N labeled gold nanoparticles for 5 h. Images were derived from confocal stacks and represent the top view (xy) as well as orthogonal slices (xz and yz). As microtubules are omitted from the nucleus, optical sectioning allows localization of this organelle (dark central region). The position of lamellar bodies can also be derived from dark circular regions not containing microtubules. The depicted Atto 647N signals correspond to two of eight positions chosen for further TEM analysis; a) position 4 and b) position 8 (see Figure 2). α-tubulin (green), Atto 647N signals (magenta).

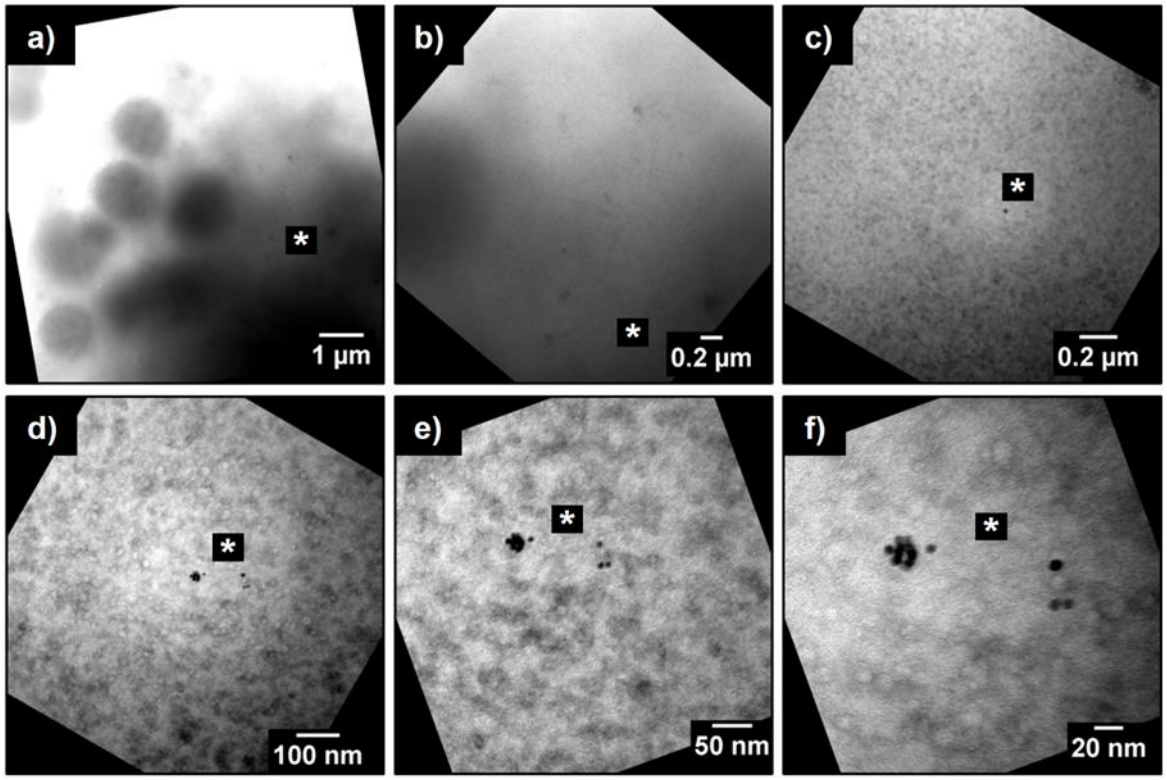

Figure 4. TEM analysis of position 4 with increasing zoom (a-f). An agglomerate of seven gold nanoparticles was detected close to a single one and three further particles. The * symbol is used to facilitate orientation within the image series and indicates the particle position in every single image. TEM images were rotated to simplify traceability. Black rims correspond to the area outside of the images.

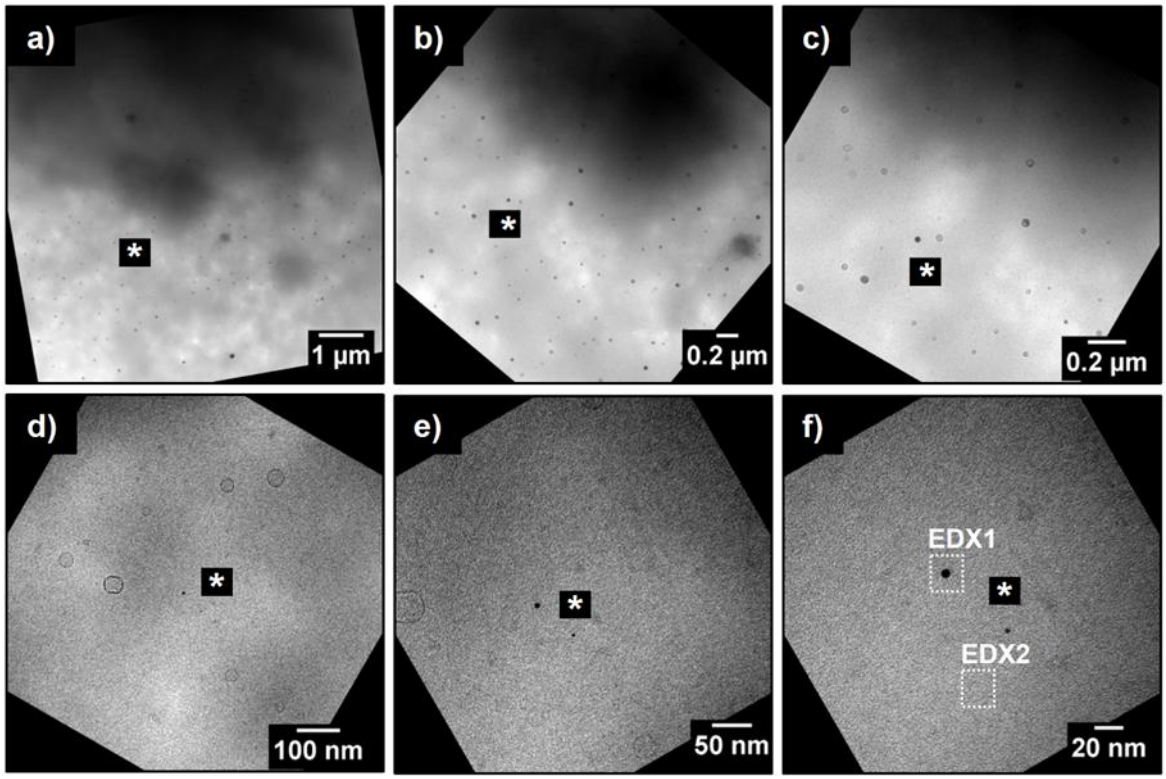

Figure 5. TEM analysis of position 8 with increasing zoom (a-f). f) Two single nanoparticles with sizes of 6 nm and 3 nm were detected. The elemental composition of the 6 nm gold particle was analyzed by EDX measurement (EDX 1, Figure S6). Circular structures already visible at lower magnification (a-c) are composed of NaCl as revealed by EDX analysis (EDX 2, Figure S6). As these structures were also visible at lower magnification (a and b), they were used as markers for the correlation of gold nanoparticles with the fluorescence signals. The formation of these structures resulted from an intermediate exposition of the dried sample to air. The * symbol is used to facilitate orientation as already explained in Figure 4. Images are rotated to simplify traceability.

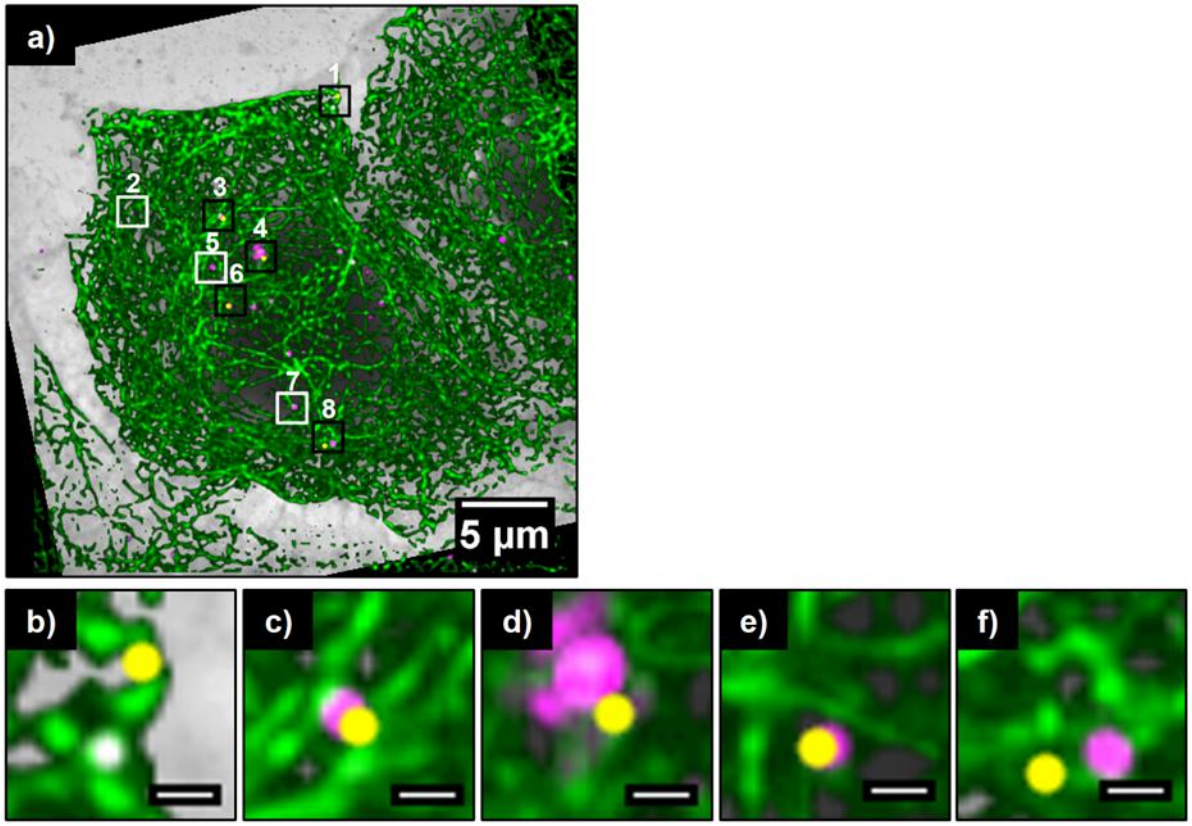

Figure 6. Correlation of the gold nanoparticles detected by TEM analysis with the Atto 647N fluorescence signals detected by CLSM. The Atto 647N fluorescence signals (magenta) at positions 1 - 8 were spatially correlated with the location of the gold particles (yellow) detected by TEM. a) Overview of the cell used for the analysis. The squares correspond to TEM images with a size of 2 µm x 2 µm. The color of the frames in a) indicates either a correlation of the Atto 647N signal with gold particles (black squares) or the lack of gold particles within that frame (white squares). b-f) Magnifications of the regions within black squares b) 1, c) 3, d) 4, e) 6, and f) 8. The Atto 647N signal in b) appears white due to its weak intensity against the background of the tubulin channel. Scale bar: 500 nm.

Table 1. Physico-chemical properties of Atto 647N labeled gold nanoparticles. d_{TEM} = particle diameter determined by TEM and image analysis. d_{DLS} = hydrodynamic particle diameter obtained by DLS measurements in water. The zeta potential of the particles was measured in water. The molar particle concentration (nM) was calculated based on a particle diameter of 8.4 nm and a gold mass concentration of 963 mg l^{-1}. λ_{Au} = absorption maximum of the particle dispersions due to the surface plasmon resonance. λ_{Abs} = absorption maximum related to coupling of Atto 647N, λ_{Em} = emission maximum of Atto 647N.

d_{TEM} [nm]	d_{DLS} [nm]	Zeta potential [mV]	Particle concentration [nM]	λ_{Au} [nm]	λ_{Ex} [nm]	λ_{Em} [nm]
8.4 ± 0.5	13.2 ± 4.8	-49.7	267	520	647	663

Table 2. Distances between Atto 647N fluorescence signals and gold nanoparticles, determined by correlation of both imaging modes. The precision of the distances corresponded to one (50 nm) and four pixel (200 nm) in the TEM images.

Position	Distances between Atto 647N signals and gold nanoparticles [nm]	Precision of the distances [+/- nm]
1	830	50
3	220	200
4	390	200
6	110	200
8	610	50

Submitted to Particle & Particle Systems Characterization

Correlative light and electron microscopy is used to detect fluorescently labeled gold nanoparticles after internalization by A549 cells. CLSM enables three-dimensional localization of fluorescence signals, whereas TEM allows for detection of gold nanoparticles. A spatial correlation of more than half of the fluorescence spots with of gold particles is found, indicating partial detachment of the labeled polymer shell.

Keywords: Fluorescence, electron microscopy, nanotoxicology, cells, nanoparticles

*Katharina Böse, Marcus Koch, Christian Cavelius, Alexandra K. Kiemer, and Annette Kraegeloh**

A Correlative Analysis of Gold Nanoparticles Internalized by A549 Cells

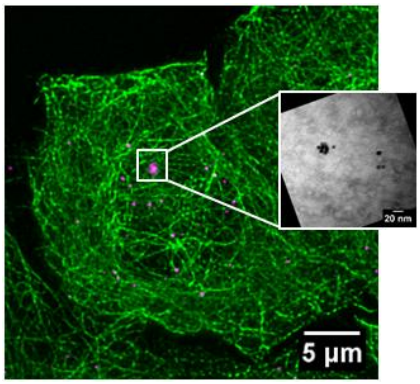

Supporting Information

for *Part. Part. Sys. Charact.*, DOI: 10.1002/ppsc.((please add manuscript number))

A Correlative Analysis of Gold Nanoparticles Internalized by A549 Cells

*Katharina Böse, Marcus Koch, Christian Cavelius, Alexandra K. Kiemer, and Annette Kraegeloh**

Gold nanoparticle synthesis

All chemicals were purchased from Sigma-Aldrich in the highest purity available and used as received unless indicated otherwise. The fluorescent dye Atto 647N-NH_2 was purchased from Atto-Tec (Germany) and stored at -20°C prior to use. Ultrapure water with a resistivity of > 18 MΩ was used for all preparation and purification steps.

Preparation of lipophilic gold particles

0.31 g (0.63 mmol) $AuPPh_3Cl$ and 313 µl (1.31 mmol) dodecanthiol were dissolved in 50 ml of toluene. After heating to 55°C, 0.54 g (6.25 mmol) tert-butylamine-borane were added under stirring. The mixture was reacted at this temperature for 60 min. The obtained gold nanoparticles were precipitated with ethanol followed by centrifugation and dispersion in 10 ml cyclohexane.

Phase transfer

100 mg of an amphiphilic polymer (Poly-maleic anhydride-alt octadecene, modified with mPEG750) were dissolved in 40 ml of water. 2 ml of lipophilic dodecanthiol-capped gold nanoparticles were added under stirring. The mixture was then emulsified for 5 min using an ultrasound disintegrator (Branson, 50% amplitude, 20 W output) and heated to 70°C to evaporate the solvent. Subsequent heating and ultrasonication yielded hydrophilic polymer-coated particles in form of a wine red transparent dispersion.

Purification and labeling

The particles were purified by centrifugation (20,000 x g) and again dispersed in water. Purification was repeated two times to remove non adsorbed polymer. The obtained dispersion was filtered into sterile falcon tubes using pyrogen-free 0.22 µm hydrophilic cellulose acetate membranes and kept sterile at 5°C.

To obtain nanoparticles with sufficient fluorescence for imaging an excess dye to nanoparticle ratio of 5,000 : 1 was chosen. After labeling, the particles were isolated by centrifugation (20,000 x g) and dispersed in water. This step was repeated until no dye fluorescence could be detected in the supernatant (3 - 4 cycles).

Characterization of gold nanoparticles

Freshly dialyzed and sterile filtered colloidal gold nanoparticle dispersions were used for characterization. The nanoparticle size, size distribution, and morphology were analyzed by TEM, using a Philips CM200 FEG (FEI Company, Eindhoven, NL) equipped with an energy dispersive X-ray (EDX) spectrometer (EDAX DX-4/Phönix, Ametek, Germany). Prior to analysis, the particle dispersion was diluted in water (1:1,000). Samples were prepared by drying the diluted nanoparticle dispersion onto a holey carbon film or a silicon nitride chip.

Particle size distributions of TEM images were obtained using the "analyze particle" tool of the ImageJ software (http://rsb.info.nih.gov/ij/). The gold concentration in aqueous dispersions was determined by inductively coupled plasma-optical emission spectroscopy (ICP-OES) with an Ultima 2 ICP-OES device (Horiba JobinYvon, Germany). A Cary 5000 spectrophotometer (Varian Inc., Germany) was used to record UV-Vis spectra of undiluted solutions in the range from 300 to 800 nm. Fluorescence spectra were recorded with a Spex FluoroMax-3 (HORIBA Scientific, Germany) using diluted (1:100) particle suspensions in MilliQ water at an excitation wavelength of 647 nm. A dye concentration of 23 ± 4 Atto 647N molecules per particle was calculated based on the particle size distribution, measured fluorescence intensity, and molar particle concentration in suspension. For dynamic light scattering experiments, a Dyna Pro Titan instrument (Wyatt Technology, Wyatt Technology Europe GmbH, Germany) with a laser wavelength of 831 nm was used to determine the hydrodynamic diameter of the particles in aqueous suspension. Prior to measurements, the gold nanoparticle suspension was filtered through a sterile 0.22 µm cellulose acetate membrane and adjusted to a nanoparticle concentration of 0.1 nM. Zeta-Potential measurements of the same suspensions were recorded using a Malvern Zetasizer Nano (Malvern, Germany).

Immunostaining of the tubulin cytoskeleton

The cells were rinsed with phosphate buffered saline (PBS) and subsequently fixed using 4 % (v/v) formaldehyde (Electron microscopy science, UK). Cells were permeabilized with 0.2 % (v/v) triton-X 100 (Roth, Germany). Blocking of unspecific antibody binding sites was carried out using 5 % (w/v) bovine serum albumin (BSA, AppliChem, Germany). α-tubulin was labeled using 1 µg ml^{-1} mouse anti-α-tubulin IgG (Invitrogen, Life Technologies, USA) and

3 µg ml^{-1} goat anti mouse Alexa 488 (Invitrogen, Life Technologies, USA) as secondary antibody. Both antibodies were diluted in 1 % (w/v) BSA. All solutions were prepared in PBS.

TEM of lipophilic 8 nm gold particles

8 nm lipophilic dodecanthiol-capped gold nanoparticles were imaged by TEM (Figure S1) prior to phase transfer and functionalization with the polymer shell. In comparison to the hydrophilic particles after phase transfer shown in Figure 1b, the coating of the particles was not visible at the edge of the carbon film by TEM.

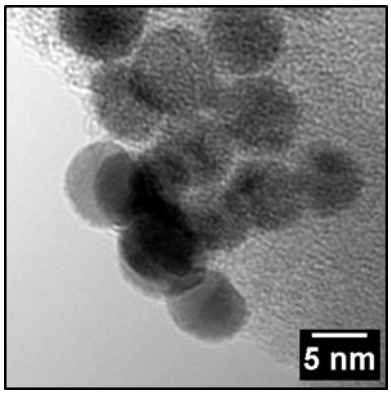

Figure S1. TEM micrograph of 8 nm gold nanoparticles without polymer shell, imaged at the edge of a holey carbon film. The carbon film is visible as the structure in the background, covering the right upper half of the image.

Spectroscopic characterization of fluorescently labeled 8 nm gold particles

Absorption and fluorescence spectra of the Atto 647N labeled gold nanoparticles were recorded (Figure S2). The absorption maximum at 520 nm was caused by the surface plasmon resonance of the gold particles. The minor signal at 647 nm was caused by Atto 647N, attached to the nanoparticle surface. The fluorescence spectrum revealed a strong emission of the nanoparticles with a maximum intensity at 663 nm.

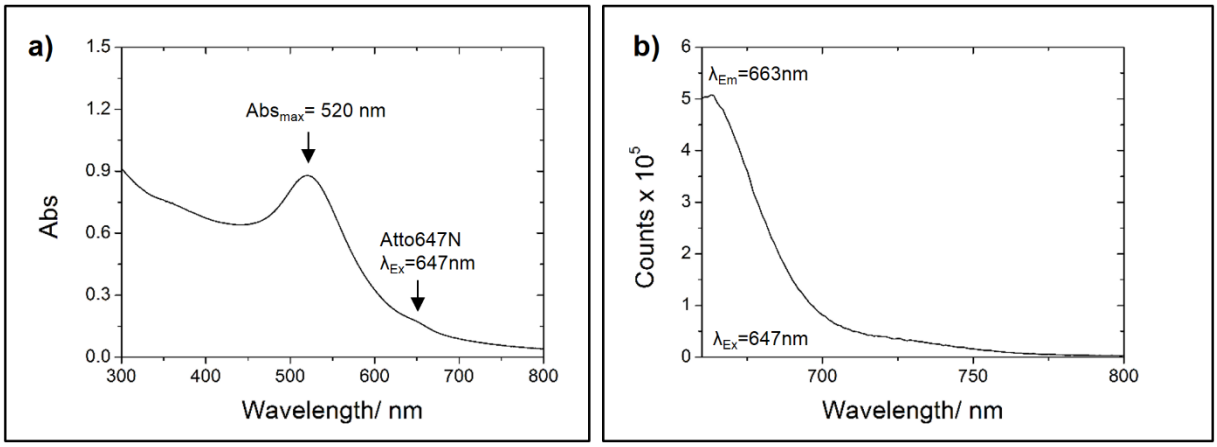

Figure S2. a) Absorption and b) fluorescence spectra of 8 nm gold nanoparticles labeled with Atto 647N.

TEM and EDX of 8 nm gold particles on silicon nitride substrates

Gold nanoparticles were deposited on silicon nitride substrates for energy dispersive X-ray (EDX) spectroscopy. The measurements confirmed that the nanoparticles consisted of gold (Figure S3). The detected Si and N signals were assigned to the silicon nitride substrate.

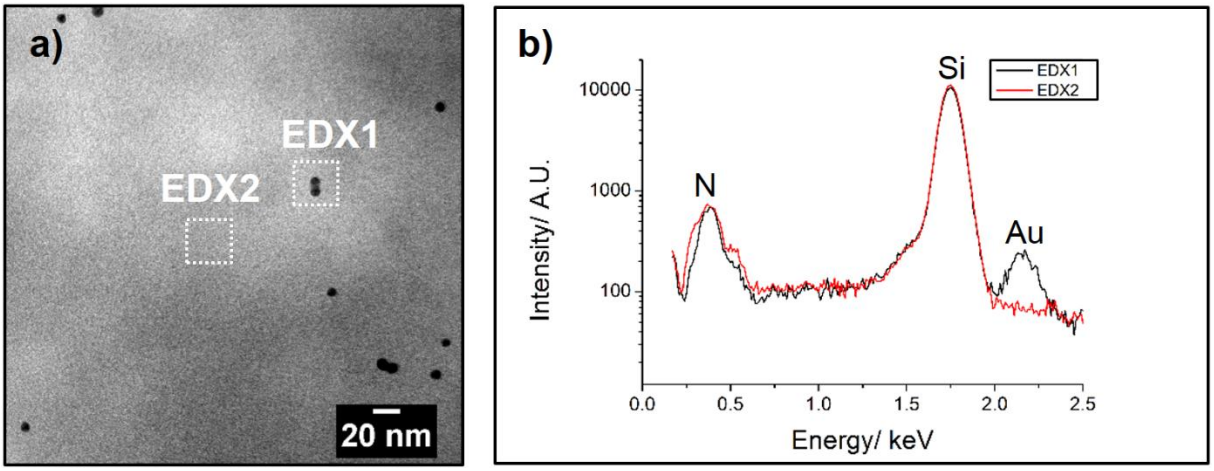

Figure S3. a) Atto 647N labeled gold nanoparticles were placed on silicon nitride chips and imaged by TEM. b) The subsequent EDX analysis allowed the identification of gold correlating with the presence of nanoparticles (EDX1) and differentiation from the substrate background (EDX2). The presence of gold was indicated by the distinctive M x-ray signal at 2.120 keV.

Internalization of 8 nm gold particles in A549 cells

Prior to the correlative analysis, the internalization of the fluorescently labeled nanoparticles by A549 cells was studied by CLSM. The Atto 647N fluorescence signal was used as indicator for the particle location. After 5 h, cell-associated Atto 647N fluorescence signals were detected. The signals were distributed in a punctate pattern, typically including signals surrounding the nucleus (Figure S4). The perinuclear location of the detected signals was indicative for the presence of the fluorescing entities inside of the cells after internalization.

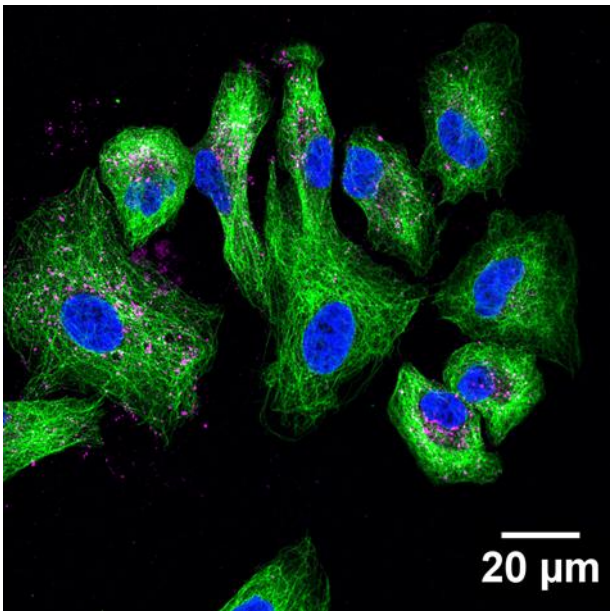

Figure S4. Image of A549 cells grown on coverslips and exposed to 0.02 µg ml^{-1} 8 nm gold nanoparticles for 5 h. α-tubulin (green), cell nucleus stained with Hoechst 33342 (blue), Atto 647N used to label the gold nanoparticles (magenta).

Distances of fluorescence signals 1 - 8 to the upper and lower margin of the cell

CLSM analysis revealed the presence of Atto 647N fluorescence signals inside A549 cells. Eight of these signals in one cell were chosen for the correlative analysis (Figure 3a). In addition, the z-position of these signals was analyzed with regard to the upper and lower margin of the cell defined by the tubulin network (Table S1, Figure 3). The axial resolution in CLSM is restricted to ≥ 500 nm, resulting in a cigar shaped point spread function. For determination of the distances, the center of the axial signals were used. The analysis was performed using the image processing package Fiji.

Table S1. Distances of Atto 647N fluorescence signals to the upper and lower margin of the cell.

Position	1	2	3	4	5	6	7	8
Distance to the apical margin [µm]	0.5	1.8	0.0	3.9	7.6	4.8	1.6	1.5
Distance to the basolateral margin [µm]	2.8	3.4	7.4	5.0	1.0	4.3	4.4	4.5

Wet STEM imaging of the cell

After CLSM analysis, the sample was transferred into the ESEM to record wet STEM images of the cell. Initially, imaging was conducted at a pressure of 750 Pa (Figure S5a and b), subsequently, the pressure was reduced to 720 Pa (Figure S5c). Based on its morphology, the cell previously imaged could be retrieved (Figure S5a). At higher magnification, dark spots were detected in the nuclear region (Figure S5b and c). At lower pressure (720 Pa), they exhibited a higher contrast. The diameter of the spot detected in c) had a diameter of about 125 nm. However, the conditions applied neither allowed for resolution of single gold nanoparticles nor identification of the material composition.

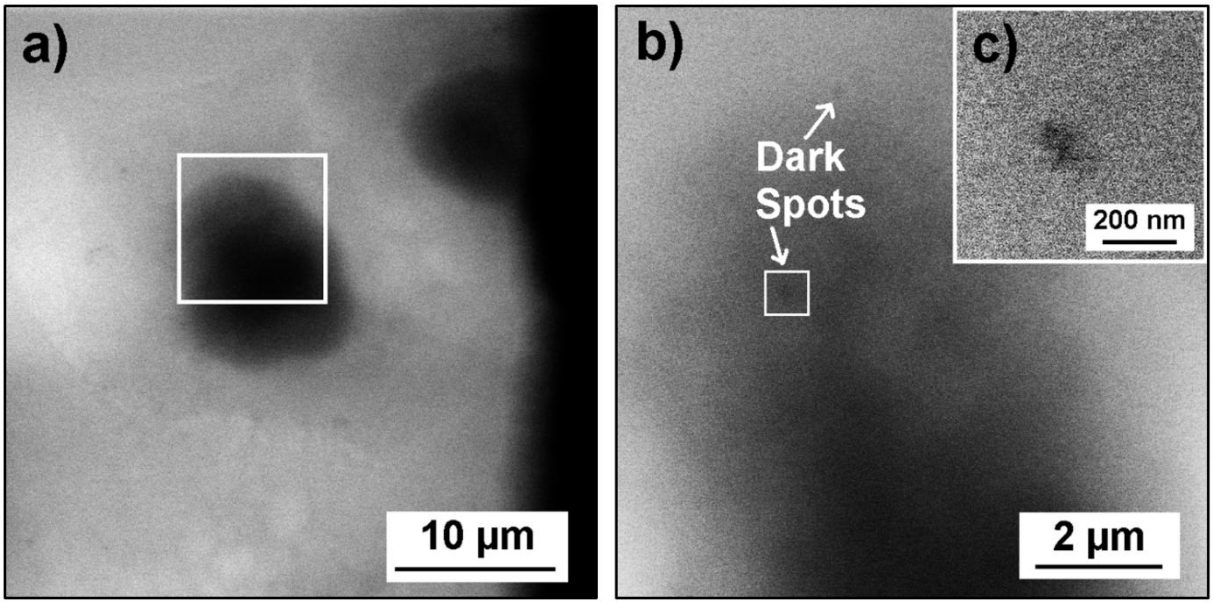

Figure S5. Wet STEM images of the cell shown in Figure 2, taken at T = 276K, E = 30 keV, a) and b) p = 750 Pa, c) 720 Pa. The squares in a) and b) indicate the magnified region in b) and c), respectively. The nucleus was visible as dark region in the center of the cell. The dark rim on the right side of the image in a) corresponded to the edge of the silicon nitride window also visible in Figure 2d. A post-fixation step was included after confocal imaging, but the samples were not exposed to contrast enhancing agents during the preparation.

EDX analyses of particles detected by TEM

EDX analyses confirmed that the particles detected at position 8 consisted of gold (Figure S6). Cu signals were generated by the sample holder; the Si and N signal by the silicon nitride substrate. C, O, S, and K signals were related to the composition of the cell.

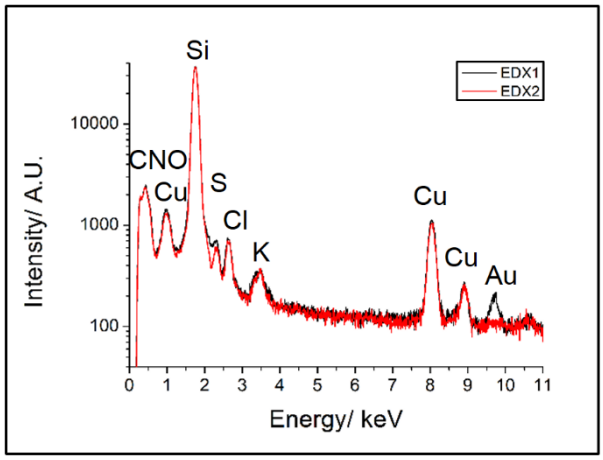

Figure S6. EDX spectra of the cell-associated gold nanoparticles detected at position 8. (EDX1) and the cellular background (EDX2) according to Figure 5. Gold was identified by means of the distinctive Lα x-ray signal (9.712 keV).

Correlation of fluorescence intensities and detected number of gold nanoparticles

By use of TEM, gold nanoparticles were identified at positions exhibiting Atto 647N fluorescence (Figure S7). The number of gold particles was compared to the fluorescence intensity detected at the same position.

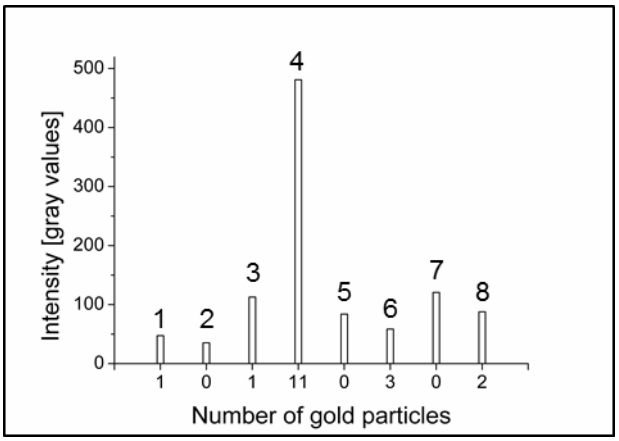

Figure S7. Number of gold nanoparticles detected by TEM compared to the fluorescence intensity at the correlative positions (1 - 8). For determination, the maximum intensity projection was used. The fluorescence intensity of the Atto 647N signals was derived by analysis of the maximal gray values using Fiji.

EDX analyses of circular structures observed by TEM

After exposition of the sample to air, circular structures formed all over the sample. Although typically not desired, these structures facilitated orientation during CLEM experiments. EDX analysis revealed that the precipitates were composed of Na and Cl (Figure S8). The Si and N signals were generated by the silicon nitride substrate.

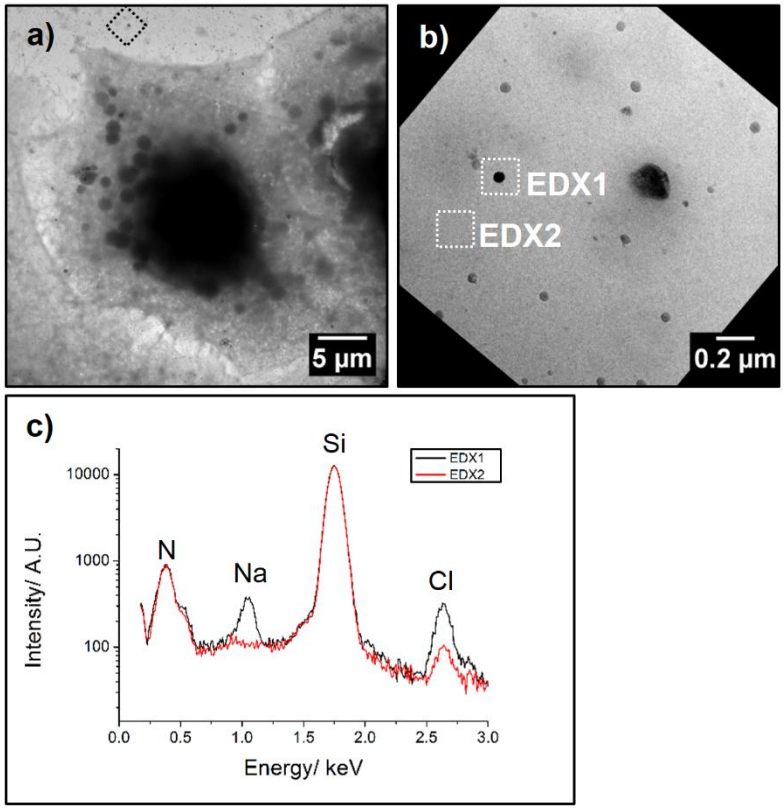

Figure S8. Circular structures, detected by TEM imaging inside and outside the cellular region, were used as markers for correlative microscopy. a) A precipitate beside the cell was chosen for detailed analysis (square). b) Magnification of the area indicated in a. c) EDX spectra of the regions labeled EDX1 and EDX2. The characteristic Kα x-ray lines of Na (1.041 keV) and Cl (2.621 keV) indicated the presence of Na and Cl within the precipitates.

Gold nanoparticle concentrations used in other microscopy studies

A concentration of 0.02 µg ml^{-1} 8 nm gold particles was used within the present work. A comparison with other microscopy related studies (Table S2) indicated that usually higher doses are applied.

Table S2. Gold nanoparticle concentrations used in other microscopy studies.

Nanoparticle size [nm]	Nanoparticle areal number density (# cm^{-2}) or nanoparticle concentration (nM)	Cell type	Cytotoxicity	Author
15	$1.5 \cdot 10^{10}$ particles·cm^{-2}	A549	n.d.	Brandenberger [3]
30	1.8·nM	Cos-7	n.d.	Peckys [30a]
18, 35, 65	10 - 100·µg·ml^{-1} ~0.01 - 2.82·nM	HDMEC	no (< 250·µg·Au ml^{-1})	Freese [30b]
8	$9.7 \cdot 10^{8}$ particles·cm^{-2} 0.0055·nM	A549	no (<·2·µg·Au ml^{-1})	This study